Radiation Hardness of dSiPM Sensors in a Proton Therapy Radiation Environment

Diblen, Faruk; Buitenhuis, Tom; Solf, Torsten; Rodrigues, Pedro; van der Graaf, Emiel; van Goethem, Marc-Jan; Brandenburg, Sytze; Dendooven, Peter

Published in:
IEEE Transactions on Nuclear Science

DOI:
10.1109/TNS.2017.2705522

Publication date:
2017

Radiation Hardness of dSiPM Sensors in a Proton Therapy Radiation Environment

Faruk Diblen, Tom Buitenhuis, Torsten Solf, Pedro Rodrigues, Emiel van der Graaf, Marc-Jan van Goethem, Sytze Brandenburg, and Peter Dendooven, *Member, IEEE*

***Abstract*— *In vivo* verification of dose delivery in proton therapy by means of positron emission tomography (PET) or prompt gamma imaging is mostly based on fast scintillation detectors. The digital silicon photomultiplier (dSiPM) allows excellent scintillation detector timing properties and is thus being considered for such verification methods. We present here the results of the first investigation of radiation damage to dSiPM sensors in a proton therapy radiation environment. Radiation hardness experiments were performed at the AGOR cyclotron facility at the KVI-Center for Advanced Radiation Technology, University of Groningen. A 150-MeV proton beam was fully stopped in a water target. In the first experiment, bare dSiPM sensors were placed at 25 cm from the Bragg peak, perpendicular to the beam direction, a geometry typical for an *in situ* implementation of a PET or prompt gamma imaging device. In the second experiment, dSiPM-based PET detectors containing lutetium yttrium orthosilicate scintillator crystal arrays were placed at 2 and 4 m from the Bragg peak, perpendicular to the beam direction; resembling an in-room PET implementation. Furthermore, the experimental setup was simulated with a Geant4-based Monte Carlo code in order to determine the angular and energy distributions of the neutrons and to determine the 1-MeV equivalent neutron fluences delivered to the dSiPM sensors. A noticeable increase in dark count rate (DCR) after an irradiation with about 10^8 1-MeV equivalent neutrons/cm^2 agrees with observations by others for analog SiPMs, indicating that the radiation damage occurs in the single photon avalanche diodes and not in the electronics integrated on the sensor chip. It was found that in the *in situ* location, the DCR becomes too large for successful operation after the equivalent of a few weeks of use in a proton therapy treatment room (about 5×10^{13} protons). For PET detectors in an in-room setup, detector performance was unchanged even after an irradiation equivalent to three years of use in a treatment room (3×10^{15} protons).**

Manuscript received December 7, 2016; revised May 2, 2017; accepted May 11, 2017. Date of publication May 18, 2017; date of current version July 14, 2017. *(Corresponding author: Peter Dendooven.)*

F. Diblen was with the KVI-Center for Advanced Radiation Technology, University of Groningen, 9747 AA Groningen, The Netherlands, and also with the Medical Imaging and Signal Processing, Department of Electronics and Information Systems, iMinds Medical IT-IBiTech, Ghent University, B-9000 Ghent, Belgium. He is now with the Netherlands eScience Center Science Park 140 (Matrix I), 1098 XG Amsterdam, The Netherlands.

T. Buitenhuis, E. van der Graaf, S. Brandenburg, and P. Dendooven are with the KVI-Center for Advanced Radiation Technology, University of Groningen, 9747 AA Groningen, The Netherlands (e-mail: p.g.dendooven@rug.nl).

T. Solf is with Philips Digital Photon Counting, 52074 Aachen, Germany.

P. Rodrigues is with Oncology Solutions, Philips Research, 5656 AE Eindhoven, The Netherlands.

M.-J. van Goethem is with the KVI-Center for Advanced Radiation Technology, University of Groningen, 9747 AA Groningen, The Netherlands, and also with the University Medical Center Groningen, Department of Radiation Oncology, University of Groningen, 9713 GZ Groningen, The Netherlands.

Color versions of one or more of the figures in this paper are available online at http://ieeexplore.ieee.org.

Digital Object Identifier 10.1109/TNS.2017.2705522

***Index Terms*— Digital SiPM, *in vivo* verification, positron emission tomography, proton therapy, radiation damage, radiation hardness.**

I. Introduction

A MAJOR advantage of proton beam radiotherapy (proton therapy), as opposed to photon beam radiotherapy, is the potential of very precise dose delivery to the tumor volume with reduced dose to healthy tissue. Due to the localized high-dose deposition, proton therapy is very sensitive to a variety of potential differences between the actual treatment situation and the one assumed during treatment planning, which may result in serious medical complications for the patient. In order to minimize the probability and severity of these complications and to have full clinical benefits of proton therapy, the dose distribution must be delivered very accurately. However, this task is difficult to achieve because of errors that may occur due to the uncertainties in proton range (as a result of uncertainties in the conversion of the planning CT Hounsfield units to proton stopping power), errors in patient setup, internal organ motion, and anatomical changes, e.g., tumor regression and weight loss, during the treatment [1]. *In vivo* verification of the delivered treatment is a way to assess this issue. Such verification allows feedback on the nature and effect on the dose of possible sources of error, allowing these errors to be corrected and the treatment plan to be adapted in order to achieve the intended total dose delivery during the remainder of the treatment.

Two main approaches, based on the detection of secondary high-energy photons, are being considered for *in vivo* dose delivery verification in proton therapy. The first approach to have been developed is positron emission tomography (PET) of the positron emitting nuclides produced by the proton beam in the patient; the second, more recently investigated, class of techniques makes use of prompt gamma rays, which are emitted on a subnanosecond timescale in the decay of excited atomic nuclei. For an overview of this subject, especially related to proton therapy, we refer to some recent reviews [2]–[8].

The past decade has seen a vigorous development of detector systems for *in vivo* dose delivery verification in proton therapy. Most often, inorganic scintillators of high density and large effective atomic number are used in order to efficiently detect the high-energy photons (511 keV in the case of PET and up to about 7 MeV in the case of prompt gamma rays). Traditionally, photomultiplier tubes (PMT) have been used

for converting the scintillation light into an electric signal. About a decade ago, Geiger-mode Avalanche Photodiodes, commonly called silicon photomultipliers (SiPM) [9]–[11], started to replace PMTs in a number of applications, including a variety of *in vivo* dose delivery verification systems [12]–[16].

Obviously, prompt gamma ray systems are installed *in situ*, i.e., near to the patient in the irradiation position, and operated while the proton beam is on. The positron emitting nuclides produced during proton therapy have relatively short half-lives (in proton therapy, ^{15}O with a half-life of 2.0 min is, generally speaking, the most important nuclide) and are subject to biological washout on a timescale comparable to the radioactive half-life [17]. Performing PET as soon as possible after the positron emitters are produced thus maximizes the total number of PET counts. PET systems are therefore preferably installed *in situ* or in-room (i.e., in the treatment room close to the irradiation position). In case of irradiations using a synchrotron accelerator, an *in situ* installation is preferred as the PET data can be acquired in between beam spills (see [16], [18]). A recent investigation into the production of very short-lived positron emitters (with half-lives from milliseconds to seconds) favors a beam-on PET implementation requiring an *in situ* installation [19]. From the considerations above, it is clear that an optimized implementation of *in vivo* dose delivery verification requires radiation detectors inside the treatment room, and in most cases close to the patient. This raises the question of the radiation hardness of the detector parts: scintillator material, photosensor, and electronics/data-acquisition components. In this respect, considering the widespread use of, or intention to use, SiPM photosensors, we consider the radiation hardness of SiPMs to be a potential showstopper for commercial deployment.

In a proton therapy environment, radiation damage mostly results from secondary neutrons produced by the proton beam, with an energy of up to 230–250 MeV, in the patient or in the beam delivery system upstream of the patient. From [20], we estimate that a detector placed perpendicularly to and at a distance of 30 cm from a 200-MeV proton beam is hit by 2×10^{-5} neutrons per cm^2 per proton stopped. In the framework of establishing the Groningen Proton Therapy Center, the number of protons delivered to one gantry treatment room was estimated to be about 10^{15} per year, assuming a realistic patient mix and a total of 380 patients. Assuming that a detector needs to operate without too large a performance degradation for at least five years, it needs to survive a total neutron bombardment of at least 10^{11} neutrons per cm^2. As the average proton beam energy used is rather around 150 MeV, this estimate can be considered as an upper limit. However, it does not include neutrons originating in the beam delivery system upstream of the patient; a nonnegligible contribution in the case of scattered beam delivery due to the presence of a collimator and bolus in the beam nozzle, close to the patient.

The literature review [21]–[31] of experiments testing the radiation hardness of SiPMs by proton or neutron irradiation, although showing differences between different devices, allows to draw some general conclusions. In most studies, particle fluences are scaled to 1-MeV neutron equivalent (n_{eq}) fluences, standard practice in this field of research. Within the proton energy range relevant for proton therapy, the scaling factor from number of protons to number of n_{eq} for damage created in silicon decreases from about 2 at 50 MeV to about 1 at 200 MeV [32], [33]. The main effect of radiation damage, starting at a fluence of about 10^8 n_{eq}/cm^2, is an increase of the leakage current (dark current) and dark count rate (DCR) that is rather linear with particle fluence. Above 10^{11} n_{eq}/cm^2, saturation of this increase has been observed. The increase in dark current/count rate has been found to be independent of the device being powered or not, bias voltage, and temperature. Single photon counting capability is lost at a fluence typically between 2×10^9 and 2×10^{10} n_{eq}/cm^2. The sensor performance in terms of gain, signal size, and photodetection efficiency suffers moderately, such that the sensor remains functional up to higher fluences, in some cases up to 10^{12} n_{eq}/cm^2, although with increased noise due to the increased DCR. The usefulness of the SiPM sensors in a radiation environment obviously depends on the particular application. Single photon counting and thus, e.g., good timing resolution (which requires time pickoff at a very low signal level), is lost rather quickly, while efficiency and energy resolution remain largely intact for a higher neutron fluence. After irradiation, sensor performance is partially recovered. The speed and amount of recovery increase when annealing at higher temperature: a 50% reduction in dark current is reached in less than a day at 60 °C [27], while a similar reduction at room temperature is reported to occur after periods from two weeks to several months. A larger recovery, however, seems to be difficult.

A recent variant of SiPMs is the so-called digital SiPM, where digitization is performed at the level of each individual microcell (SPAD, single-photon avalanche diode). Examples are sensors developed by Philips Digital Photon Counting (PDPC) [34] and the SPADnet collaboration [35]. Advantages over analog SiPMs are the perfect scaling of performance with total sensor surface area of a system and the fact that poorly performing SPADs can be switched off individually.

We report here on the first investigation of the radiation hardness in a proton therapy environment of the PDPC dSiPM sensors and PET detectors based on these sensors. We mimicked the situation of *in situ in vivo* dose delivery verification in proton therapy by irradiating the sensors with neutrons produced in the stopping of high-energy protons in water. In addition, the energy and angular distributions of the neutrons produced were studied using Monte-Carlo simulations.

II. Methods

A. dSiPM Sensors and dSiPM-Based PET Detectors

dSiPM tile sensors from PDPC [36] were used in the experiments. A tile sensor has an outer dimension of 32.6×32.6 mm^2 and consists of 16 individual DPC3200 sensor dies, arranged in a 4×4 matrix. Each sensor die consists of a 2×2 matrix of pixels with each pixel containing 3200 SPADs (microcells) of dimension 59.4×64 μm^2. The pixels are further divided into four subpixels. The 16 sensor dies operate individually by running through a configurable event acquisition sequence,

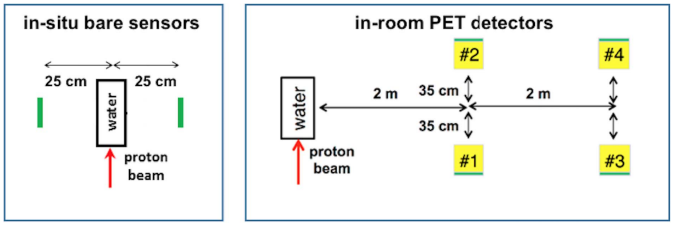

Fig. 1. Position of the dSiPM sensors and dSiPM-based PET detectors with respect to the proton beam and water target for *in situ* (left) and in-room geometries (right). The drawings are schematic and not to scale.

which is started by an internal trigger. Data acquisition dead time and accepted dark-count noise events can be controlled by configurable trigger schemes (related to the average number of detected photons) and validation schemes (related to the geometrical distribution of SPAD discharges on a pixel). The trigger scheme refers to the number of individual subpixels of a pixel that must see at least one discharge in order to generate a valid trigger. Trigger scheme 2 corresponds to a discharge within any two of the four subpixels, whereas trigger scheme 4 requires that all four subpixels of a pixel see a discharge in order to generate a valid trigger. More details can be found in [34] and [37].

In order to investigate the effect of radiation on the performance of time-of-flight-PET detectors, dSiPM-based PET detectors were irradiated. The detectors consisted of an 8×8 array of $3.8 \times 3.8 \times 22$ mm^3 lutetium yttrium oxyorthosilicate (LYSO) scintillation crystals coupled one-to-one to the pixels of the dSiPM tile sensor.

B. Irradiation Setups

Radiation hardness experiments were performed at the irradiation facility of the AGOR cyclotron at the KVI-Center for Advanced Radiation Technology, University of Groningen. A 150-MeV proton beam was fully stopped in a $35 \times 28 \times 18$ cm^3 water target. The proton beam entered the target in the middle of a side face. As the size and the concrete walls of the irradiation room are not unlike those of a proton therapy treatment room (they are designed for a proton beam energy of 190 MeV), the experiments were done in a radiation environment that is very similar to that of a typical proton therapy irradiation, both with respect to direct radiation from the target as well as radiation scattered from walls, floor, and ceiling.

In the first experiment, bare dSiPM tile sensors were placed at 25 cm from the Bragg peak, perpendicular to the beam direction [Fig. 1 (left)], a geometry typical for the *in situ* implementation of a PET or prompt gamma imaging device.

In a second experiment, pairs of dSiPM-based PET detectors were placed with a distance of 70 cm between them at 2 and 4 m from the Bragg peak, perpendicular to the beam direction [Fig. 1 (right)]; a situation resembling the in-room implementation of a typical commercial PET scanner. A fifth detector was placed behind a 1-m thick concrete wall inside the irradiation room, at a distance of about 4 m and an angle of about 110° with respect to the proton beam, allowing to judge the effect of some in-room concrete shielding.

In the first experiment, seven successive irradiations were performed, such that the cumulative number of protons increased in logarithmic steps from a number corresponding to a typical therapy fraction (3×10^{11} protons) up to a treatment room operation of 12 months (1×10^{15} protons). A beam current of 50 nA was used. Radiation damage was assessed by the increase in DCR. Before the experiment, the DCR of each of the about 2×10^5 microcells of a tile sensor was measured. After each irradiation, the DCR of each microcell was measured again and the ratio with the DCR measured before the experiment calculated. For display purposes, the DCR ratios were then ordered from low to high values. Accelerated testing in which a certain radiation dose is delivered in a much shorter time, thus using a much higher dose rate, compared with the application being investigated is, for practical reasons, widely used. It is, however, a worst case scenario: compared with irradiation over a longer time, it does not allow for a potential amount of damage repair by annealing and thus recovery of the sensor. The DCR ratio distribution after the sensor was stored at room temperature for three weeks after the irradiation was measured in order to assess the recovery potential.

In the second experiment, an irradiation equivalent to three years of operation (3×10^{15} protons) was delivered in 110 min (average proton beam current of 73 nA). The performance of the PET detectors after the experiment was compared with the performance before irradiation. These measurements were performed in a climate chamber at a temperature of 5 °C in order to reduce the DCR of the dSiPM sensors.

C. Monte Carlo Simulation of Neutron Spectra

The purpose of the Monte Carlo simulations was to obtain detailed information on the angular and energy distribution of the neutrons produced during the irradiations. A software framework based on the Geant4 toolkit, version 10.0.1 [38], was set up. The experimental arrangement of the water target relative to the proton beam was accurately implemented. An infinitely narrow monoenergetic 150-MeV beam was used to irradiate the target. The omission of the experimental beam width (about 5-mm full-width-at-half-maximum) and energy spread (a few 100 keV) is a valid approximation considering the accuracy aimed at. The angle and energy of the neutrons leaving the water target are scored on a spherical surface with 1-m radius and centered at the center of the target.

III. Results

A. In Situ dSiPM Sensors

The ratio of the DCR after and before irradiation for bare dSiPM tile sensors as measured during the first experiment is shown in Fig. 2. The DCR is measured sequentially for each of the about 2×10^5 microcells. In order to limit the duration of a DCR measurement, the DCR of each microcell is measured for a short time only, ranging from 65 ms for the unirradiated sensor to 6.5 ms after the final irradiation. These measurement times reflect a compromise between measurement duration and statistical accuracy. Microcells with a

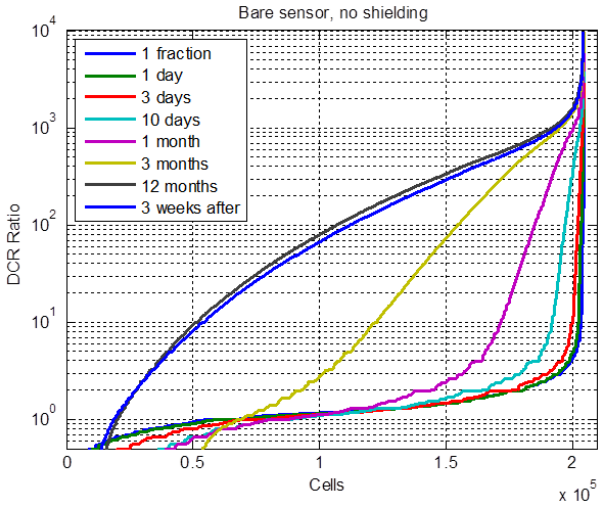

Fig. 2. DCR ratios for bare dSiPM sensors located at 25 cm from the Bragg peak, perpendicular to the beam direction. On the horizontal axis, the microcells are ordered from lowest to highest DCR ratio. Curves for different durations of operation of a treatment room are shown. The "12-months" operation corresponds to 10^{15} protons. The "three weeks after" curve shows a small recovery due to room temperature storage for three weeks after the irradiation.

low DCR show a relatively large variation in measured DCR due to Poisson statistics, and as a result, the DCR ratios of these microcells can be lower than 1, as shown in Fig. 2. In addition, some microcells give 0 counts within the short measurement interval and thus result in a DCR ratio of 0. These two effects of low counting statistics, in combination with the decreasing DCR measurement times for successive irradiation steps, explain the somewhat erratic behavior of the DCR ratio curves in Fig. 2 (bottom-left). Included in Fig. 2 is the DCR ratio measured after three weeks of room temperature storage after the irradiation, showing a small recovery (25% reduction in total DCR) of the radiation damage.

B. In-Room PET Detectors

The mean and median of the DCR distribution, expressed in counts/s per cell, before and after an irradiation equivalent to three years of operation of a treatment room (3×10^{15} protons) for the different PET detector locations [see Fig. 1 (right)] are shown in Fig. 3. Location 5 refers to the detector behind a concrete wall inside the irradiation room.

Table I compares the performance of the PET detectors before and after irradiation. Trigger schemes 2 and 4 correspond to an average threshold of 2.3 and 8.3 microcells fired. A lower number trigger scheme provides better coincidence resolving time (CRT), but at the expense of a reduced counting efficiency for 511-keV photons. The latter follows from the fact that a lower number trigger scheme results in a higher rate of triggers generated by dark counts. These triggers keep the detector readout busy, i.e., they induce dead time, reducing the availability for detecting true signals (511-keV photons in this case) and thus reducing the counting efficiency.

C. Neutron Spectra

Fig. 4 presents the simulated neutron energy spectra for different angles with respect to the direction in which the

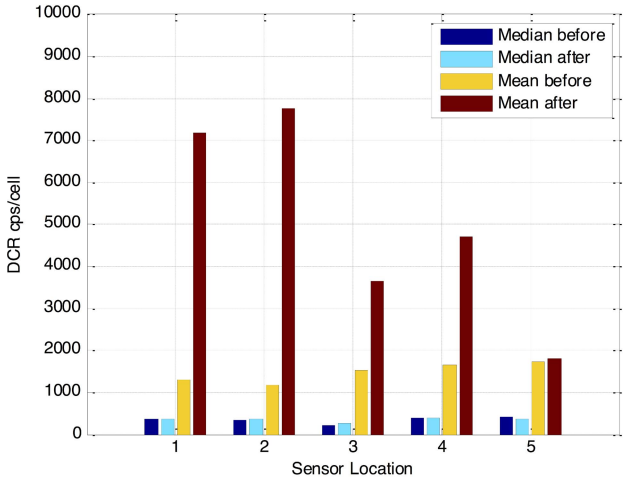

Fig. 3. Mean and median DCR (counts/s per microcell) before and after irradiation of in-room dSiPM-based PET detectors.

TABLE I

COMPARISON OF THE PERFORMANCE OF PET DETECTORS BEFORE AND AFTER IRRADIATION. THE ENERGY RESOLUTION AT 511 keV ($\Delta E/E$), CRT, AND NUMBER OF COUNTS MEASURED USING TRIGGER SCHEME 2 RELATIVE TO THE NUMBER OF COUNTS MEASURED USING TRIGGER SCHEME 4. AFTER IRRADIATION, MEASUREMENTS WERE DONE WITH 90% AND 80% OF MICROCELLS WITH THE LOWEST DCR ENABLED. FOR THE DETECTORS AT 2 AND 4 m, THE ENERGY RESOLUTION OF BOTH DETECTORS IS GIVEN

before/after irradiation	enabled cell fraction [%]	ΔE/E [%]	CRT [ps]	relative counts [%]
detectors at 2 m				
before	90	11.2 / 11.3	306	95
after	90	11.2 / 11.3	304	56
after	80	11.5 / 11.4	309	91
detectors at 4 m				
before	90	11.7 / 12.0	310	89
after	90	11.7 / 12.7	315	80
after	80	12.7 / 12.8	335	95
detectors behind concrete wall				
before	90	11.6	308	89
after	90	11.6	306	86
after	80	11.8	328	97

protons travel. In order to increase the statistics from the simulation, the values given for the forward and backward angles (0° and 180°) were obtained by integration over the 0–5 and 175°–180° intervals. For the other angles, the simulation results were integrated over an interval of ±5° around the central values which are given. The well-known decrease in neutron energy and intensity with angle is clearly seen. The large values at 1 MeV (representing all neutrons below 1 MeV) are mostly due to thermal neutrons.

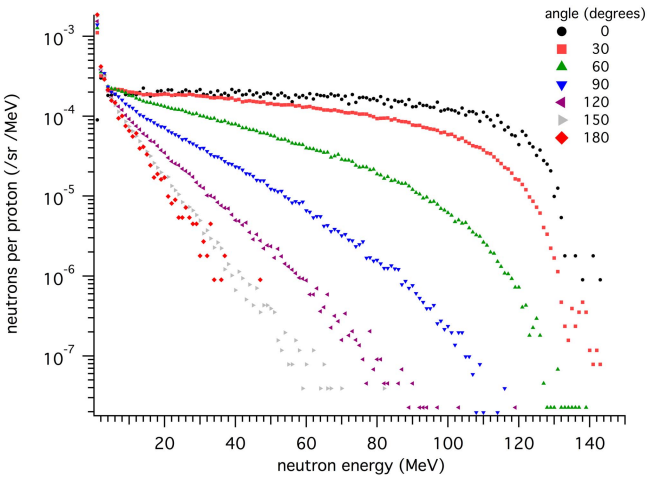

Fig. 4. Neutron energy spectra for different angles with respect to the proton beam direction (0° corresponds to the direction in which the protons travel). The spectra are normalized per incident proton and per solid angle.

IV. Discussion

A decreased counting efficiency after irradiation is seen for the PET detectors at 2 and 4 m from the target when operated using trigger scheme 2 (right column of Table I). This is due to the fact that the increased DCR in combination with a low trigger threshold causes triggers due to dark counts, inducing dead time and thus reducing the availability for detecting true signals. This effect is substantially larger for the detectors at 2 m than those at 4 m. The counting efficiency can, however, be recovered by reducing the rate of triggers induced by dark counts by switching off an additional 10% of the microcells with the highest DCR. The counting efficiency of the detectors installed behind the concrete wall inside the irradiation room does not suffer appreciably and switching off additional microcells to recover efficiency is not needed.

In order to compare our results on the DCR increase of the bare dSiPM sensors in an *in situ* geometry with the general picture that emerges from the literature (see Section I), the neutron energy spectra shown in Fig. 4 were characterized in terms of 1-MeV neutron equivalent fluences following the procedure described in [39]. Reference [39] gives the damage versus neutron energy up to 20 MeV; for higher energies [32, Fig. 2] was used. The 1-MeV neutron equivalent fluences were integrated over the neutron energy range. In this, the first data point of Fig. 4, representing neutrons with an energy below 1 MeV, was not included as it contains mostly neutrons with an energy far below 1 MeV, for which the damage relative to that at 1 MeV is very small. Table II gives the 1-MeV equivalent neutron fluences per proton versus angle with respect to the proton beam, both per steradian and per cm^2 at a distance of 25 cm (representing a solid angle of 1.6×10^{-3} sr), the distance used in the experiments.

Fig. 2 shows a noticeable increase in the DCR after an irradiation equivalent to a few days of operation of a treatment room. The three-day equivalent number of protons is about 10^{13}. Following Table II for an angle of 90°, this corresponds to about 10^8 n_{eq}/cm^2. This is in agreement with the literature, where the DCR starts to increase at a fluence of about 10^8 n_{eq}/cm^2. The dSiPM sensors thus behave not unlike their analog counterparts, indicating that the radiation damage occurs in the SPADs, not in the electronics integrated on the sensor chip.

TABLE II

1-MeV Equivalent Neutron Fluences (n_{eq}) per Proton Versus Angle With Respect to the Proton Beam, per Steradian, and per cm^2 at a Distance of 25 cm, the Distance Used in the Experiments

angle	n_{eq}/sr	n_{eq}/cm^2
0	3.09×10^{-2}	4.94×10^{-5}
30	2.43×10^{-2}	3.89×10^{-5}
60	1.30×10^{-2}	2.08×10^{-5}
90	6.72×10^{-3}	1.08×10^{-5}
120	4.07×10^{-3}	6.51×10^{-6}
150	3.16×10^{-3}	5.06×10^{-6}
180	2.93×10^{-3}	4.69×10^{-6}

V. Conclusion

For dSiPM sensors in an *in situ* location, DCRs become too large for successful operation after a few weeks of use in a treatment room (Fig. 2). A small recovery at room temperature of radiation damage on a time scale of weeks was observed, which is insufficient to significantly alter the sensor survival time. For dSiPM-based PET detectors in an in-room location, the median DCR is quite unaffected after three years of use in a treatment room (Fig. 3). This is due to the fact that the radiation damage causes a large increase in the DCR in only a small number of microcells. Disabling these damaged microcells mitigates the effect of the damage without compromising PET detector performance (see Table I).

We conclude that unshielded dSiPM sensors in an *in situ* location suffer from a significant increase in DCRs due to neutron radiation damage. The digital infrastructure of the sensor was not permanently affected by any of the described tests, but high DCRs create dead time and therefore sensitivity loss in a potential *in situ* application. It was shown that sensors located a few meters from the patient during irradiation show a very moderate increase in the DCR. Essential is the unique possibility of dSiPM sensors to disable damaged microcells in order to mitigate radiation damage. Therefore, PET performance is expected to stay constant for over three years of clinical operation when using automated re-calibration of the SPAD sensor arrays.

References

[1] H. Paganetti, "Range uncertainties in proton therapy and the role of Monte Carlo simulations," *Phys. Med. Biol.*, vol. 57, no. 11, pp. R99–R117, 2012.

[2] M. T. Studenski and Y. Xiao, "Proton therapy dosimetry using positron emission tomography," *World J. Radiol.*, vol. 2, no. 4, pp. 135–142, 2010.

[3] K. Parodi, "*In vivo* dose verification," in *Proton Therapy Physics*, H. Paganetti, Ed. Boca Raton, Fl, USA: CRC Press, 2011, pp. 489–524.

[4] F. Fiedler, D. Kunath, M. Priegnitz, and W. Enghardt, "Online irradiation control by means of PET," in *Ion Beam Therapy*, U. Linz, Ed. Berlin, Germnay: Springer-Verlag, 2012, pp. 527–543.

[5] X. Zhu and G. El Fakhri, "Proton therapy verification with PET imaging," *Theranostics*, vol. 3, no. 10, pp. 731–740, 2013.

[6] A.-C. Knopf and A. Lomax, "*In vivo* proton range verification: A review," *Phys. Med. Biol.*, vol. 58, no. 15, pp. R131–R160, 2013.

[7] A. C. Kraan, "Range verification methods in particle therapy: Underlying physics and Monte Carlo modeling," *Frontiers Oncol.*, vol. 5, 2015, Art. no. 150.

[8] K. Parodi, "Vision 20/20: Positron emission tomography in radiation therapy planning, delivery, and monitoring," *Med. Phys.*, vol. 42, no. 12, pp. 7153–7168, Dec. 2015.

[9] B. Dolgoshein *et al.*, "Status report on silicon photomultiplier development and its applications," *Nucl. Instrum. Methods Phys. Res. A, Accel. Spectrom. Detect. Assoc. Equip.*, vol. 563, no. 2, pp. 368–376, Jul. 2006.

[10] D. Renker and E. Lorenz, "Advances in solid state photon detectors," *J. Instrum.*, vol. 4, no. 4, p. P04004, 2009.

[11] S. Korpar, "Status and perspectives of solid state photon detectors," *Nucl. Instrum. Methods Phys. Res. A, Accel. Spectrom. Detect. Assoc. Equip.*, vol. 639, no. 1, pp. 88–93, May 2011.

[12] I. Perali *et al.*, "Prompt gamma imaging of proton pencil beams at clinical dose rate," *Phys. Med. Biol.*, vol. 59, no. 19, pp. 5849–5871, 2014.

[13] Y. Shao *et al.*, "In-beam PET imaging for on-line adaptive proton therapy: An initial phantom study," *Phys. Med. Biol.*, vol. 59, no. 13, p. 3373, 2014.

[14] P. Solevi *et al.*, "Performance of MACACO Compton telescope for ion-beam therapy monitoring: First test with proton beams," *Phys. Med. Biol.*, vol. 61, no. 14, pp. 5149–5165, 2016.

[15] P. C. Lopes *et al.*, "First *in situ* TOF-PET study using digital photon counters for proton range verification," *Phys. Med. Biol.*, vol. 61, no. 16, pp. 6203–6230, 2016.

[16] M. A. Piliero *et al.*, "Full-beam performances of a PET detector with synchrotron therapeutic proton beams," *Phys. Med. Biol.*, vol. 61, no. 23, pp. N650–N666, 2016.

[17] K. Grogg *et al.*, "Mapping ^{15}O production rate for proton therapy verification," *Int. J. Radiat. Oncol. Biol. Phys.*, vol. 92, no. 2, pp. 453–459, Jun. 2015.

[18] W. Enghardt *et al.*, "Charged hadron tumour therapy monitoring by means of PET," *Nucl. Instrum. Methods Phys. Res. A, Accel. Spectrom. Detect. Assoc. Equip.*, vol. 525, nos. 1–2, pp. 284–288, 2004.

[19] P. Dendooven *et al.*, "Short-lived positron emitters in beam-on PET imaging during proton therapy," *Phys. Med. Biol.*, vol. 60, no. 23, pp. 8923–8947, 2015.

[20] A. K. Biegun *et al.*, "Time-of-flight neutron rejection to improve prompt gamma imaging for proton range verification: A simulation study," *Phys. Med. Biol.*, vol. 57, no. 20, pp. 6429–6444, 2012.

[21] A. H. Heering *et al.*, "Radiation damage studies on SiPMs for calorimetry at the super LHC," in *Proc. Conf. Rec. IEEE NSS*, Oct. 2008, pp. 1523–1526.

[22] P. Bohn *et al.*, "Radiation damage studies of silicon photomultipliers," *Nucl. Instrum. Methods Phys. Res. A, Accel. Spectrom. Detect. Assoc. Equip.*, vol. 598, no. 3, pp. 722–736, Jan. 2009.

[23] L. Carrara, C. Niclass, N. Scheidegger, H. Shea, and E. Charbon, "A gamma, X-ray and high energy proton radiation-tolerant CIS for space applications," in *IEEE ISSCC Dig. Tech. Papers*, Feb. 2009, pp. 40–41 and 41a.

[24] T. Matsumura *et al.*, "Effects of radiation damage caused by proton irradiation on multi-pixel photon counters (MPPCs)," *Nucl. Instrum. Methods Phys. Res. A, Accel. Spectrom. Detect. Assoc. Equip.*, vol. 603, no. 3, pp. 301–308, May 2009.

[25] Y. Musienko, D. Renker, Z. Charifoulline, K. Deiters, S. Reucroft, and J. Swain, "Study of radiation damage induced by 82 MeV protons on multi-pixel Geiger-mode avalanche photodiodes," *Nucl. Instrum. Methods Phys. Res. A, Accel. Spectrom. Detect. Assoc. Equip.*, vol. 610, no. 1, pp. 87–92, 2009.

[26] S. S. Majos *et al.*, "Noise and radiation damage in silicon photomultipliers exposed to electromagnetic and hadronic radiation," *Nucl. Instrum. Methods Phys. Res. A, Accel. Spectrom. Detect. Assoc. Equip.*, vol. 602, no. 2, pp. 506–510, Apr. 2009.

[27] Y. Qiang, C. Zorn, F. Barbosa, and E. Smith, "Radiation hardness tests of SiPMs for the JLab Hall D Barrel calorimeter," *Nucl. Instrum. Methods Phys. Res. A, Accel. Spectrom. Detect. Assoc. Equip.*, vol. 698, pp. 234–241, Jan. 2013.

[28] M. Andreotti *et al.*, "Study of the radiation damage of silicon photomultipliers at the GELINA facility," *J. Instrum.*, vol. 9, no. 4, p. P04004, 2014.

[29] Y. Musienko, A. Heering, R. Ruchti, M. Wayne, A. Karneyeu, and V. Postoev, "Radiation damage studies of silicon photomultipliers for the CMS HCAL phase I upgrade," *Nucl. Instrum. Methods Phys. Res. A, Accel. Spectrom. Detect. Assoc. Equip.*, vol. 787, pp. 319–322, Jul. 2015.

[30] Z. Li *et al.*, "Characterization of radiation damage caused by 23 MeV protons in multi-pixel photon counter (MPPC)," *Nucl. Instrum. Methods Phys. Res. A, Accel. Spectrom. Detect. Assoc. Equip.*, vol. 822, pp. 63–70, Jun. 2016.

[31] A. Heering, Y. Musienko, R. Ruchti, M. Wayne, A. Karneyeu, and V. Postoev, "Effects of very high radiation on SiPMs," *Nucl. Instrum. Methods Phys. Res. A, Accel. Spectrom. Detect. Assoc. Equip.*, vol. 824, pp. 111–114, Jul. 2016.

[32] G. Lindström, "Radiation damage in silicon detectors," *Nucl. Instrum. Methods Phys. Res. A, Accel. Spectrom. Detect. Assoc. Equip.*, vol. 512, nos. 1–2, pp. 30–43, Oct. 2003.

[33] A. Akkerman, J. Barak, M. B. Chadwick, J. Levinson, M. Murat, and Y. Lifshitz, "Updated NIEL calculations for estimating the damage induced by particles and γ-rays in Si and GaAs," *Rad. Phys. Chem.*, vol. 62, no. 4, pp. 301–310, Oct. 2001.

[34] Y. Haemisch, T. Frach, C. Degenhardt, and A. Thon, "Fully digital arrays of silicon photomultipliers (dSiPM)—A scalable alternative to vacuum photomultiplier tubes (PMT)," *Phys. Procedia*, vol. 37, pp. 1546–1560, 2012.

[35] C. Bruschini *et al.*, "SPADnet: Embedded coincidence in a smart sensor network for PET applications," *Nucl. Instrum. Methods Phys. Res. A, Accel. Spectrom. Detect. Assoc. Equip.*, vol. 734, pp. 122–126, Jan. 2014.

[36] *Philips Digital Photon Counting*, accessed on Jun. 20, 2017. [Online]. Available: http://www.digitalphotoncounting.com

[37] T. Frach, "Optimization of the digital silicon photomultiplier for cherenkov light detection," *J. Instrum.*, vol. 7, C01112, 2012.

[38] J. Allison *et al.*, "Geant4 developments and applications," *IEEE Trans. Nucl. Sci.*, vol. 53, no. 1, pp. 270–278, Feb. 2006.

[39] *Standard Practice for Characterizing Neutron Energy Fluence Spectra in Terms of an Equivalent Monoenergetic Neutron Fluence for Radiation-Hardness Testing of Electronics*, ASTM Standard E722, ASTM International, West Conshohocken, PA, USA, 2004.